Supplemental material to the paper

"Magnetoconductance, Quantum Hall Effect, and Coulomb Blockade in Topological Insulator Nanocones"

Raphael Kozlovsky, Ansgar Graf, Denis Kochan, Klaus Richter, Cosimo Gorini[1]

[1] *Institut für Theoretische Physik, Universität Regensburg, 93040 Regensburg, Germany*

(Dated: March 20, 2020)

NUMERICAL IMPLEMENTATION

Kwant takes as an input tight-binding Hamiltonians of nanostructures and applies the so-called wave function approach to compute their electronic transport properties using the Landauer-Büttiker formalism [39]. Tight-binding Hamiltonians are passed to kwant as "conventional" Hermitian matrices, i.e. finite dimensional matrices which fulfill $(H^*)^T = H$. However, discretizing the continuum Hamiltonian Eq. (2) leads to a tight-binding representation which does not fulfill this condition. Let us clarify that the reason for this is the non-trivial (non-constant, i.e. coordinate dependent) volume form. Consider, for simplicity, a one-dimensional system with real space coordinate q and volume form $\mathrm{d}V = g(q)dq$. On the lattice, we use the shorthand notation $g_i \equiv g(q_i)$ as well as $\Psi_i \equiv \Psi(q_i)$, where i labels the lattice sites. The condition for the Hermiticity of H, $\langle\Phi|H\Psi\rangle = \langle H\Phi|\Psi\rangle$, is then given by

$$\sum_{ij} g_i \Phi_i^* H_{ij} \Psi_j = \sum_{ij} g_j \left(H_{ji}\Phi_i\right)^* \Psi_j \tag{7}$$

on the lattice. From Eq. 7, it is, in general, only possible to deduce that $(H^*)^T = H$ if $g(q) = \text{const}$. Hence, we use the local transformation

$$H \to \tilde{H} = \sqrt{g(q)} H (1/\sqrt{g(q)}), \tag{8}$$

$$\Psi \to \tilde{\Psi} = \sqrt{g(q)}\Psi \tag{9}$$

which makes the volume form trivial. This can be easily seen by considering the scalar product

$$\langle\Phi|H\Psi\rangle = \int_{-\infty}^{\infty} \mathrm{d}q\, g \Phi^* H \Psi \tag{10}$$

$$= \int_{-\infty}^{\infty} \mathrm{d}q\, (\sqrt{g}\Phi^*) \left(\sqrt{g} H \frac{1}{\sqrt{g}}\right) (\sqrt{g}\Psi) \tag{11}$$

$$= \int_{-\infty}^{\infty} \mathrm{d}q\, \tilde{\Phi}^* \tilde{H} \tilde{\Psi}. \tag{12}$$

Note that in Eq. 12, g is fully absorbed in the wave functions and the Hamiltonian, the volume form is trivial. Hence, using the transformation Eq. 8 yields a tight-binding Hamiltonian $\tilde{H}$ which fulfills $(\tilde{H}^*)^T = \tilde{H}$.

We implement the magnetic fields via usual Peierls phases and consider standard Gaussian-correlated disorder,

$$\langle V(\mathbf{r}) V(\mathbf{r}')\rangle = K \frac{\hbar v_F}{2\pi\xi^2} e^{-|\mathbf{r}-\mathbf{r}'|^2/2\xi^2}, \tag{13}$$

with disorder strength K and correlation length ξ. For our simulations we use $K = 0.1$ and $\xi = 7$ nm. To avoid the fermion doubling problem [25, 26], we use a conventional Wilson mass term. For a recent discussion see Ref. [27]. Note that a Wilson mass affects the specifics of the spin-momentum texture. Such specifics are, however, irrelevant for our charge transport problem.

EFFECTIVE MASS POTENTIAL FOR THE TI NANOCONE IN WEAK COAXIAL MAGNETIC FIELD

In order to develop a feeling of how the effective potential $|V_l(s,B)|$ defined in Eq. (6) affects transport, we consider the conductance through a clean TINC (with the same geometry as in Fig. 3) for zero and weak coaxial magnetic field without doping in the leads.

The conductance for $B = 0$ as a function of the Fermi energy ϵ_F, depicted in Fig. 5 (a), shows equidistant conductance steps of size $2e^2/h$. Their position and height can be explained with the corresponding effective potentials, which are plotted in Fig. 5(b) for all l-values which are relevant in the depicted energy range. The central region in between the black vertical lines (600 nm $\leq s \leq$ 1200 nm) corresponds to the truncated cone, while the regions $s < 600$ nm and $s > 1200$ nm correspond to straight leads. The leads are modeled by semi-infinite cylindrical nanowires, thus $|V_l(s,B)|$ is constant. Note that for $B = 0$, the effective potential $|V_l(s)| \propto |l + 0.5|/R(s)$ is purely determined by the finite size confinement energy, hence the spacing in the left lead (smaller circumference), is larger than in the right lead (larger circumference). Modes which enter the scattering region (the truncated cone) via the leads are described by a well defined orbital angular momentum quantum number l, and each of them feels the effective potential $|V_l(s)|$. As soon as the Fermi energy surpasses the effective potential for a given l, the corresponding mode has enough energy to traverse the TINC and a step in the conductance appears. Since there is no disorder and modes are twofold degenerate in

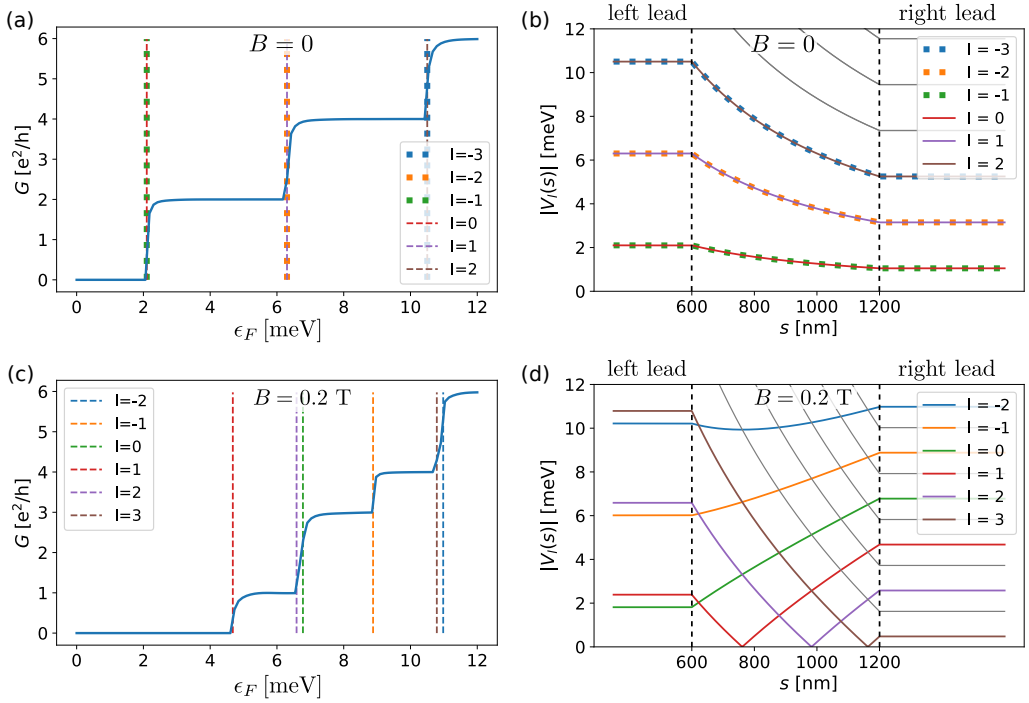

FIG. 5. Conductance as a function of Fermi energy (left panels) and effective potentials (right panels) for a clean TI nanocone with leads, see Fig. 1(c). Panels (a) and (b) correspond to $B = 0$, panels (c) and (d) to a coaxial magnetic field $B = 0.2$ T. Steps in the conductance appear whenever the Fermi energy ϵ_F surpasses one of the effective potentials $|V_l(s, B)|$ labeled by l (corresponding energies are marked by vertical lines). For the conductance simulations we used *kwant* and a Fermi velocity of $v_F = 5 \times 10^5$ m/s.

orbital momentum, the conductance is quantized in units of $2e^2/h$.

In Fig. 5 (c) and Fig. 5 (d), the conductance and the effective potential for a coaxial magnetic field of $B = 0.2\,\mathrm{T}$ is shown. For low energies $\lesssim 2$ meV, the characteristic effective potential "wedges", ubiquitous in Fig. 3(b) (strong magnetic field $B = 2\,\mathrm{T}$), start to emerge. In the conductance, a more complicated step sequence appears with step sizes of e^2/h and $2e^2/h$ since orbital angular momentum degeneracy is broken due to the magnetic flux. The first step in the conductance, which is of size e^2/h, appears at ≈ 4.75 meV which corresponds to the opening of the $l = 1$ mode [red curve in (d)]. Modes with $l = 0$ (green curve) and $l = 2$ (purple curve) appear almost at the same energy around 6.75 meV. The proximity of those two mode openings leads to a step size in the conductance of $2e^2/h$.

Note that due to rotational symmetry, modes cannot change their orbital angular momentum quantum number l. However, as soon as rotational symmetry is broken, for instance, by disorder, modes couple. This coupling forms the basis of the resonant transport through Dirac LLs (consisting of bound states of effective potential wedges) discussed in the main manuscript.

SMOOTHED TI NANOCONE

For the description of a smoothed TINC we choose to work with the coaxial coordinate z. We approximate the Heaviside step function by $\Theta_\sigma(z - z') = \frac{1}{2} + \frac{1}{\pi}\arctan[\sigma(z - z')]$, $\lim_{\sigma\to\infty} \Theta_\sigma(z - z') = \Theta(z - z')$. The radius of a junction that starts with a cylinder of radius R_0 at $z = -\infty$ and becomes a cylinder of radius R_1 at $z = \infty$ with an intermediate smoothed TINC can then be written as

$$\begin{aligned} R_\sigma(z) =& R_0 + (R_1 - R_0)\Theta_\sigma(z - z_1) \\ &+ \mathcal{S}(z - z_0)[\Theta_\sigma(z - z_0) - \Theta_\sigma(z - z_1)], \end{aligned} \tag{14}$$

where $\mathcal{S} = (R_1 - R_0)/(z_1 - z_0)$ is the slope of a TINC with initial radius R_0, final radius R_1 and length $z_1 - z_0$. The input parameters chosen for Fig. 4 are such that in the limit $\sigma \mapsto \infty$ the function (14) agrees with the TINC studied in Fig. 3. Thus $R_0 = C_{\min}/(2\pi) = 78.3\,\mathrm{nm}$, $R_1 = 2R_0 = C_{\max}/(2\pi) \approx 156.6\,\mathrm{nm}$, $z_0 = 0$ and $z_1 = 594.7\,\mathrm{nm}$.